PHASE-ENCODED, RAPID, MULTIPLE-ECHO (PERME) NUCLEAR MAGNETIC RESONANCE IMAGING

Mark Steven Lawton
Master of Engineering Thesis

August 1985

ACKNOWLEDGEMENTS

ABSTRACT

The importance of producing quality NMR images at high speed has led to numerous proposals for RF-pulse and magnetic field gradient sequences. The k-space formulation of NMR imaging is utilized to introduce a new high-speed, high-resolution imaging sequence. The new sequence, **PERME** imaging, features speed and resolution without the need for any new data processing nor new requirements on hardware (such as rapidly switched gradients or extreme homogeneity).

PERME imaging utilizes multiple spin echoes to map a k-space rectilinear grid in non-sequential order. Non-sequential sampling and timing delays yield a favorable k-space transfer function. The transfer function describes the attenuation of spatial frequencies. In producing a 16x16 pixel image, using four RF-induced echoes, PERME imaging samples lines 1,5,9,13 in the first FID. Lines 2,6,10,14 are sampled in the second FID. Non-sequential sampling continues until the 16 line rectilinear grid is sampled in four FIDs. Extension to higher resolution images is straightforward.

A simulation package which utilizes the k-space formulation is used to compare and contrast the PERME method against the widely used spin-warp method. The simulation generates the complex NMR signal for phantoms with analytically calculable Fourier transforms and a range of T_2s consistent with those in biological samples.

The simulation demonstrates that the point-spread-function (PSF) of PERME imaging in the phase encoding direction resembles the Lorentzian line shape. Results indicate that the PSFs for 2 and 4 echo PERME imaging yield images without artifacts. Thus PERME imaging may establish itself as a legitimate high-speed alternative to spin-warp imaging.

INTRODUCTION

Over the past several years a myriad of NMR imaging schemes have been proposed and implemented. A common aspect of all methods is the desire to encode spatial information in each free induction decay (FID). There are three basic categories for two-dimensional NMR imaging: 1) Echo-planar[1] techniques encode enough spatial information in one FID to make an entire image. These methods feature high speed while suffering from poor signal to noise ratio, image artifacts due to insufficient sampling, and defects due to reconstruction algorithms poorly matched to the actual gradient waveforms used[2]. 2) Projection techniques (spin-warp[3], projection reconstruction[4], Fourier zeugmatography[5], etc.) encode a fraction of the required spatial information in each FID. In producing images with high resolution and minimal artifacts these methods require data collection over a period of typically 10 to 20 minutes. 3) Selective region methods (for example the sensitive point technique[6]) encode only one region of spatial information into each FID. These three categories represent a wide spectrum in terms of both total data acquisition time and image quality.

This paper introduces a novel imaging scheme which is a compromise in imaging time but not image quality between echo-planar techniques and projection techniques. This new method, **P**hase-**E**ncoded, **R**apid, **M**ultiple-**E**cho (**PERME**) imaging, can produce images similar to those of the widely used spin-warp method in 1/2 to 1/4 the total number of FIDs. Thus, PERME imaging establishes itself as a *hybrid* between the high speed echo-planar techniques and the high resolution projection techniques.

In order to compare and contrast PERME imaging to other methods it is beneficial to understand the relationship of the spatial frequency content of an object to the NMR imaging experiment. This relationship is elucidated by the k-space trajectory formulation of the NMR imaging process[7,8,9].

K-SPACE ANALYSIS

Any NMR imaging sequence can be understood as a realization of sampling a discrete set of points in k-space. K-space is a Hilbert space in which an object is described by its spatial frequency representation. K-space is related to "object " space by the n-dimensional Fourier transform. This can be seen by examining the equation for the NMR signal after detection in quadrature.

Assuming all spins within the object are on-resonance then the complex NMR signal voltage after a uniform B_1 pulse is proportional to:

$$S(t) = \int e^{-t/T_2(\mathbf{r})} \rho(\mathbf{r}) \, e^{i\Phi(\mathbf{r},t)} \, d\mathbf{r}.$$

$\rho(\mathbf{r})$ is the distribution of transverse magnetization throughout the volume, $T_2(\mathbf{r})$ is the spatially varying spin-spin relaxation constant, and $\Phi(\mathbf{r},t)$ is given by:

$$\Phi(\mathbf{r},t) = \mathbf{r} \, \gamma \int \mathbf{G}(t') \, dt'.$$

$\mathbf{G}(t')$ is the time dependent magnetic field gradient vector and γ is the gyromagnetic ratio. Let,

[1]
$$\mathbf{k}(t) = \gamma \int \mathbf{G}(t') \, dt'$$

then $\Phi(\mathbf{r},t)$ is given by the vector inner product,

$$\Phi(\mathbf{r},t) = \mathbf{r} \, \mathbf{k}(t)$$

and

[2]
$$S(t) = \int e^{-t/T_2(\mathbf{r})} \rho(\mathbf{r}) \, e^{i\mathbf{r}\,\mathbf{k}(t)} d\mathbf{r}.$$

If T_2 is constant throughout the sample then,

[3]
$$S(t) = e^{-t/T_2} \left[\int \rho(\mathbf{r}) \, e^{i\mathbf{r}\,\mathbf{k}(t)} d\mathbf{r} \right]$$

If $\mathbf{k}(t)$ is the vector whose components $[k_x(t), k_y(t), k_z(t)]$ represent spatial frequencies then, by definition, the term in brackets is the Fourier transform of the transverse magnetization. The NMR signal can then be rewritten as:

$$S(t) = e^{-t/T_2} F[\mathbf{k}(t)]$$

where the function $F[\mathbf{k}]$ is the spatial Fourier transform of the transverse magnetization.

Thus, *the complex NMR signal at any time is proportional to the value of the spatial Fourier transform of the magnetization* at the point in k-space given by $[k_x(t), k_y(t), k_z(t)]$ where $k_j(t)$ is the integral over time of the linear magnetic field gradient in the jth direction. That is, as time progresses the magnetic field gradients trace out a trajectory in k-space. As the trajectory is traversed the NMR signal varies as different values of the function $F[\mathbf{k}]$ are sampled.

Figure 1 shows a basic pulse sequence utilizing magnetic field gradients and the corresponding trajectory which it traces out in k-space. Because the pulse sequence does not include a z gradient $k_z(t)=0$; the trajectory remains in the k_x-k_y plane (the plane of the paper).
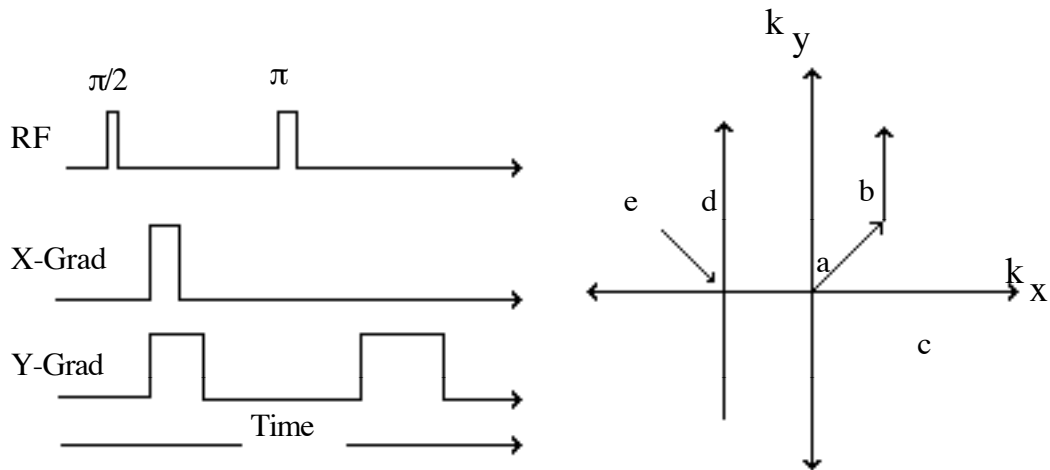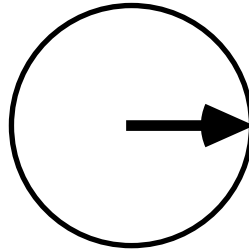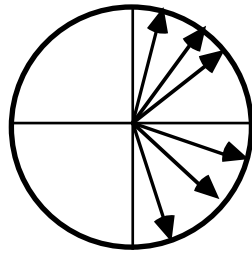

FIGURE 1
Relationship between pulse sequence and k-space trajectory.

a) Simultaneous application of y (dephasing) gradient and x (phase-encoding) gradient.
b) Application of y gradient only.
c) Effect of a π pulse.
d) Application of y (readout) gradient.
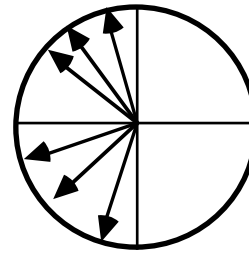e) Echo peak occurs when crossing axis.

As shown in figure 1, a π pulse simply alternates the trajectory to the opposite quadrant of k-space. This alteration reflects the fact that the Fourier transform of real functions have positive and negative frequencies which are complex conjugates. Because $\rho(\mathbf{r})$ is a real function, opposite quadrants of k-space are complex conjugate pairs. This fact is further detailed in figure 2.

a) Initial magnetization.

b) Spins before π pulse.

c) Spins after π pulse.

$S(t_b)$ $=$ signal before π pulse

$S(t_b)$ $=$ $e^{-t_b/T_2} \int \rho(\mathbf{r}) e^{i\Phi(\mathbf{r},t_b)} d\mathbf{r}$

$=$ $e^{-t_b/T_2} F[\mathbf{k}(t_b)]$

$=$ $- e^{-t_a/T_2} \int \rho(\mathbf{r}) e^{-i\Phi(\mathbf{r},t_b)} d\mathbf{r}$

$S(t_a)$ $=$ signal after π pulse

$S(t_a)$ $=$ $e^{-t_a/T_2} \int \rho(\mathbf{r}) e^{i\Phi(\mathbf{r},t_a)} d\mathbf{r}$

$=$ $e^{-t_a/T_2} \int \rho(\mathbf{r}) e^{i[\pi-\Phi(\mathbf{r},t_b)]} d\mathbf{r}$

$=$ $e^{-t_a/T_2} \int \rho(\mathbf{r}) e^{i\pi} e^{-i\Phi(\mathbf{r},t_b)} d\mathbf{r}$

$=$ $- e^{-t_a/T_2} F^*[\mathbf{k}(t_b)]$

$=$ $- e^{-t_a/T_2} F[-\mathbf{k}(t_b)]$

FIGURE 2

Effect of a π pulse on k-space coordinates.

a) Magnetization after $\pi/2$ excitation pulse.
b) Spins dephase as a result of gradients and inhomogeneities.
c) Spins retain phase information after π pulse.
* indicates complex conjugate.

The signal after the π pulse is the negative complex conjugate of the signal before the π pulse. Because the spin distribution, $\rho(\mathbf{r})$, is a real function F[$\mathbf{k}$] is the complex conjugate of F[-$\mathbf{k}$].   Therefore a π pulse corresponds to moving to the opposite quadrant of k-space and inverting the polarity of the signal.

Each complex valued measurement taken by the digitizer during acquisition corresponds to the spatial Fourier transform of the object at some point along the k-space trajectory. Imaging schemes (spin-warp, projection reconstruction, echo-planar, etc.) differ only in the trajectories used to sample k-space and the manner of transforming the k-space data back to object space to generate an image[7].

The following facts are of importance in all imaging schemes. 1) Despite the fact that the Fourier transform is a continuous function in k-space it can only be sampled at a finite number of points. 2) Associated with each imaging scheme is a transfer function which describes the attenuation of spatial frequencies. Some spatial frequencies lie beyond the region of k-space which is sampled in the imaging experiment. These frequencies do not get represented in the final image. Thus, the transfer function, H[$\mathbf{k}$], is zero at these frequencies. Spatial frequencies which do lie in the region of k-space sampling are attenuated due to the decaying NMR signal. The transfer function at these frequencies is decreased because of this attenuation. The effect of the transfer function on the image is the convolution of the object with a kernel which is the Fourier transform of the transfer function. Indeed, the progress of NMR imaging can be attributed to the fact that the convolution kernels of most imaging schemes are of minor detriment. That is, only a small fraction of the signal power in a given pixel is due to signal convolved in from other areas. As seen in figure 3 the two factors which determine the transfer function are the trajectory and the rate of signal decay due to T_2 relaxation.

Trajectory   Transfer Function

FIGURE 3
K-space trajectories and transfer functions[7] for
common imaging schemes.

T_2 relaxation causes spatial frequencies to be attenuated. Because only a finite region of k-space can be sampled in the NMR experiment some spatial frequencies do not get sampled. The transfer function is zero exterior to the sampling region.

PERME IMAGING

The imaging scheme described in this paper is a novel pulse sequence which samples the same points of k-space as the widely used spin-warp imaging method. However the strategy for mapping k-space is very much different in that multiple lines of k-space are sampled in each FID. Thus the total imaging time is reduced by a factor of n (the number of echoes used). The fact that PERME imaging samples k-space on a rectilinear grid means that the transformation from k-space to object space is simply a matter of using a 2D Fourier transformation routine. That is, no additional data processing is required. The key to the high speed of PERME imaging is the use of multiple individually encoded spin-echoes in mapping k-space[10]. As an example, consider the trajectories required to produce a 16x16 pixel image for the spin-warp method and a 4-echo PERME sequence. Spin-warp imaging samples one line of k-space in each of 16 FIDs. PERME imaging samples four lines of k-space in each FID. The order of sampling is as follows: lines 1,5,9,13 are sampled in the first FID. Lines 2,6,10,14 are sampled in the second FID. Non-sequential sampling continues as shown in table I until the 16 line rectilinear grid is sampled in only four FIDs. Figure 4 shows the trajectories during data acquisition for both methods.

FID	Echo 1	Echo 2	Echo 3	Echo 4
1	1	5	9	13
2	2	6	10	14
3	3	7	11	15
4	4	8	12	16

TABLE I
Order of k-space sampling for a 16x16
PERME image using 4 echoes.

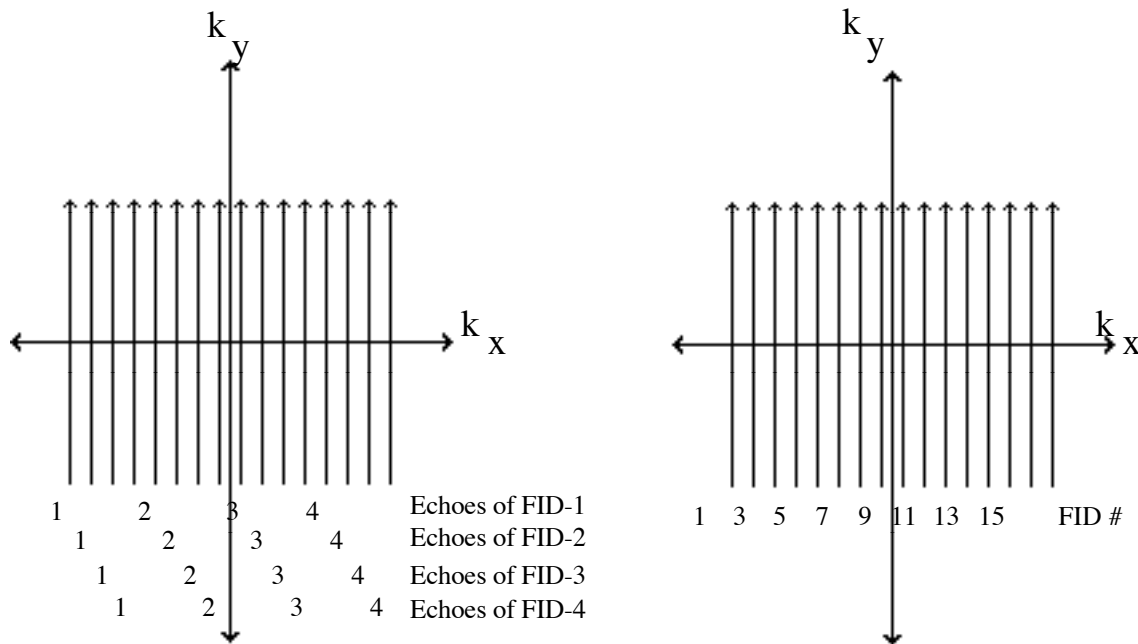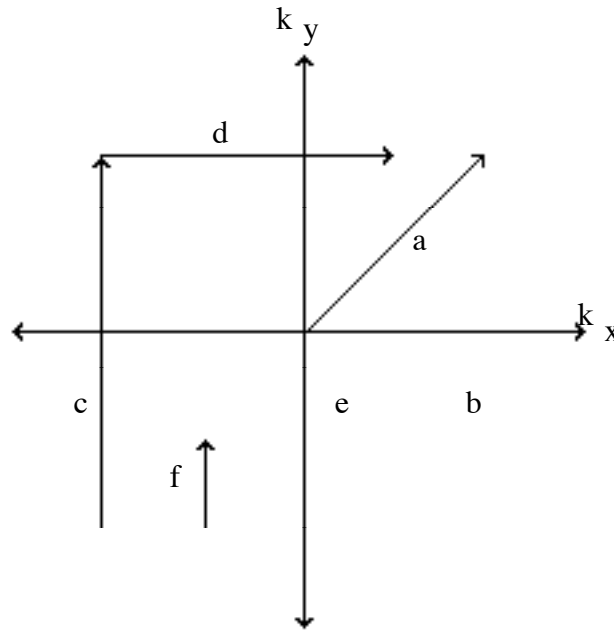1 & 16 correspond to $-k_x$ max and $+k_x$ max respectively.

FIGURE 4
K-space sampling for 16x16 pixel images.

Figure 4 shows only the path traversed during data acquisition. To move from the origin of k-space to the start of data acquisition, PERME imaging utilizes a combination of phase encoding gradients, a dephasing pulse, and π pulses.   As an example, figure 5 shows the path taken to move from the origin, through the first echo and data acquisition, to the start of acquisition for the second echo.

FIGURE 5
K-space trajectory from the origin to the start of the second acquisition
for first FID of a 16x16 pixel PERME image using 4 echoes.

a) Simultaneous application of dephasing gradient and first phase encoding gradient.
b) First π pulse.
c) First readout gradient and data acquisition (k-space line 1).
d) Second phase encoding gradient.
e) Second π pulse.
f) Beginning of second readout gradient and data acquisition (k-space line 5).

As stated above, all imaging schemes have a transfer function which describes the attenuation of spatial frequencies. The transfer functions for spin-warp and PERME imaging are shown in figure 6. Examining the PERME transfer function it is interesting to note that the signal from the point which suffers the worst attenuation due to T_2 relaxation (point 2) is the complex conjugate of the signal from the point which suffers the least attenuation (point 1). A similar situation is true of all points in between (for example points 3 and 4). Thus some "signal averaging" is inherent in this method.

PERME Imaging   Spin-warp Imaging

FIGURE 6
K-space transfer functions.

PERME imaging samples complex conjugate pairs early and late in T_2 decay. The PERME transfer function differs in that it has an exponential decay in the k_x direction.

The equations for the transfer functions are:

[4]   Spin-warp: $H(k_x, k_y) = e^{-\Delta t/T_2} = e^{-(k_y+k_y')/(\gamma G_y T_2)}$

[5]   PERME: $H(k_x, k_y) = \left[e^{-(k_y+k_y')/(\gamma G_y T_2)}\right]\left[e^{-(k_x+k_x') TE N_e D/(2\pi T_2 N_x)}\right]$

Δt	=	Time elapsed since start of acquisition.
T_2	=	Spin-spin relaxation constant.
k_x'	**=**	Maximum value of k-space sampled in k_x direction.
k_y'	**=**	Maximum value of k-space sampled in k_y direction.
γ	=	Gyromagnetic ratio.
G_y	=	Gradient strength (gauss/centimeter).
TE	=	Echo time.
N_e	=	Number of echoes.
D	=	Size of imaging area in x direction.
N_x	=	Number of pixels in x direction.

In both methods there is an exponential decay in the k_y direction as a result of using a readout gradient to translate k-space in the k_y direction. The difference between the spin-warp transfer function and the PERME transfer function is the exponential decay in the k_x direction for the PERME method. The cause of the exponential decay can be seen by examining the pulse sequence.

PULSE SEQUENCE

The pulse sequence for PERME imaging using 4 echoes is shown in figure 7. The important fact to notice in this pulse sequence is that before each π pulse the x-gradient is turned on to provide new phase encoding. The phase encoding gradients are chosen to sample k-space in the non-sequential manner described above.
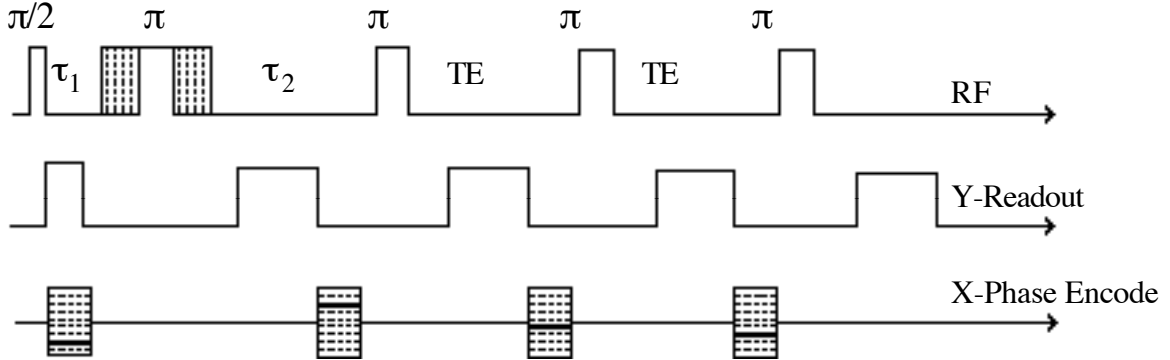

FIGURE 7
Pulse sequence.

For each successive FID, the time before the first π pulse (τ_1) and the time between the first and second π pulses (τ_2) is increased. Phase encoding gradients are chosen to sample the appropriate lines of k-space. The timing delays in conjunction with the appropriate choice of k-space sampling yields an exponential decay in the k-space transfer function associated with T_2 relaxation.

In addition to non-sequential k-space sampling, PERME imaging introduces timing delays into the pulse sequence. For each successive FID, the time before the first π pulse (τ_1) and the time between the first and second π pulses (τ_2) is increased. These incremental delays cause each line of k-space to be sampled at a different point in the decay of the signal. Because the delays are incremented in constant steps and the phase encoding gradients are chosen to sample k-space in non-sequential order, the resulting k-space transfer function profile in the k_X direction is exponential. The amount of delay for a 16x16 PERME image is given in table II.

FID	Total Delay	Echo 1	Echo 2	Echo 3	Echo 4
1	0	1	5	9	13
2	$1\Delta T^*$	2	6	10	14
3	$2\Delta T$	3	7	11	15
4	$3\Delta T$	4	8	12	16

TABLE II
K-space sampling and timing delays for a 16x16 pixel PERME image using 4 echoes.

* $\Delta T = TE/4$

Extension to higher resolution images is straightforward. For example, for a 64x64 image, lines 1,17,33,49 are sampled in the first FID. The second FID samples lines 2,18,34,50. The order of k-space sampling and the amount of delay for higher resolution images is found using the following equations:

$$\text{k-space line sampled} = \text{FID \#} + (\text{Echo \#} - 1)(N_x/N_e)$$

$$\text{total delay} = \Delta(\tau_1 + \tau_2) = (\text{FID \#} - 1)(\text{TE } N_e / N_x)$$

where: N_x = Number of pixels in x direction.

N_e = Number of echoes used.

TE = Echo time.

The order of k-space sampling in conjunction with the timing delays, provides a smooth exponential decay in the k-space transfer function. The decay is caused by T_2 relaxation.

To eliminate the possibility of new artifacts due to chemical shift or B_o inhomogeneities it is necessary that τ_1 and τ_2 be incremented in equal steps. Thus any additional phase shift due to inhomogeneities or chemical shift which occurs during τ_1 gets refocussed during τ_2.

In addition, care must be taken to store data from each echo in the appropriate row of the 2 dimensional data matrix before Fourier transformation. For example, data from the 5th line of k-space must be stored in the 5th row of the data matrix.

Finally it is important that the following criterion be observed in generating the pulse sequence. The area under the y-gradient dephasing pulse must equal one-half of the area under the y-gradient readout pulse. This causes the magnitude of the k_y coordinate to be the same before and after the readout gradient. That is, $|k_y|$ after acquisition $= |k_y|$ before acquisition. This insures that the only difference in phase between acquisitions is due to the phase encoding gradients. Thus the integrity of the rectilinear grid is maintained.

SIMULATION

A simulation package has been written that can simulate the complex NMR signal that would be received, after quadrature detection, from phantoms consisting of rectangles and ellipses of any intensity and any orientation. The simulation uses the k-space theory outlined above to generate and inverse Fourier transform the complex NMR signal. The simulation consists of three main blocks: generation of points in k-space, generation of the NMR complex signal and Fourier inversion. Figure 8 shows a flow chart which outlines the simulation package.
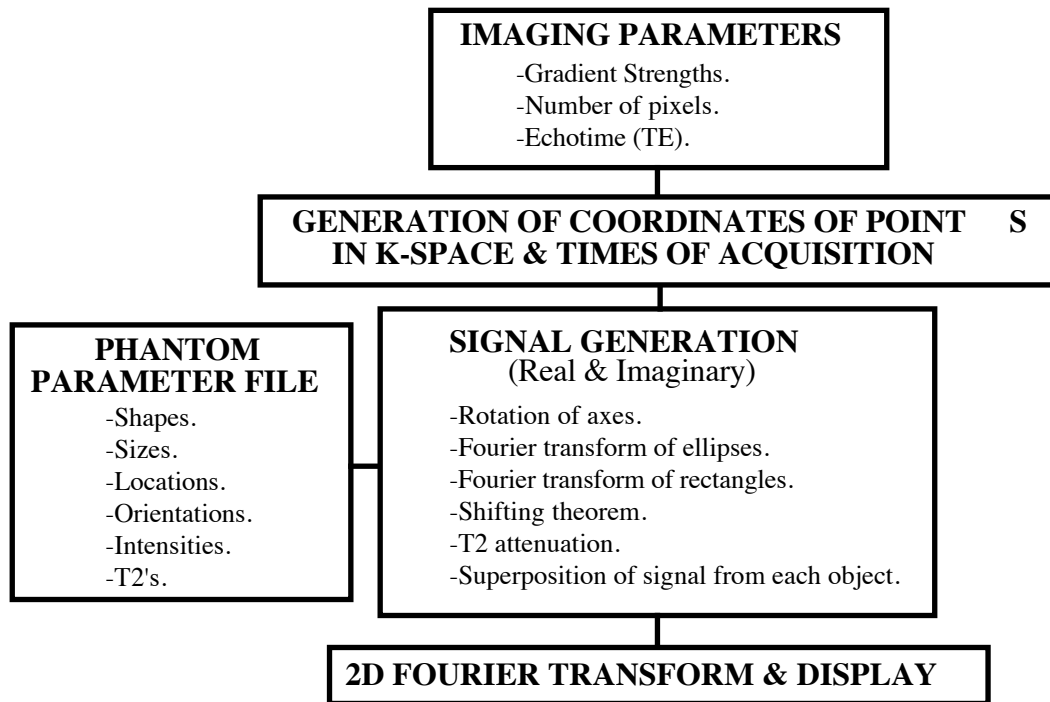

IMAGING PARAMETERS
-Gradient Strengths.
-Number of pixels.
-Echotime (TE).

GENERATION OF COORDINATES OF POINTS IN K-SPACE & TIMES OF ACQUISITION

PHANTOM PARAMETER FILE
-Shapes.
-Sizes.
-Locations.
-Orientations.
-Intensities.
-T2's.

SIGNAL GENERATION
(Real & Imaginary)
-Rotation of axes.
-Fourier transform of ellipses.
-Fourier transform of rectangles.
-Shifting theorem.
-T2 attenuation.
-Superposition of signal from each object.

2D FOURIER TRANSFORM & DISPLAY

FIGURE 8
Simulation flow chart.

As discussed above the points sampled in k-space are dependent on the trajectory. The trajectory is purely a function of the RF-pulse and magnetic field gradient sequence. Both spin-warp and PERME imaging sample k-space on a rectilinear grid as shown in figure 4. The equations that generate the coordinates of each point in k-space are (from equation 1):

$$k_x(t) = \gamma \int G_x(t') \, dt'$$

$$k_y(t) = \gamma \int G_y(t') \, dt'$$

$$k_z(t) = 0.$$

(The simulation assumes the use of a z-gradient only for slice selection, thereby setting $k_z(t) = 0$.)

The k-space coordinates are used to generate the simulated NMR signal data (real and imaginary components). The simulation simply computes the value of the Fourier transform of the phantom at each point in k-space given by $(k_x(t), k_y(t))$. The total Fourier transform at each point is the sum of the contributions from each rectangle and ellipse. The Fourier transforms of a rectangle and ellipse of known intensities and dimensions are:

rectangle: $F(k_x, k_y) = 4$ intensity $[\sin(k_x \text{ width}) \sin(k_y \text{ length})]/(k_x k_y)$

ellipse: $F(k_x, k_y) = 2$ intensity (major axis)(minor axis) $J_1(A)/A$.

$J_1(A)$ is a first order Bessel function and $A = [(k_x \text{ major axis})^2 + (k_y \text{ minor axis})^2]^{1/2}$. If an object is not centered at the origin its Fourier transform is given by the shifting theorem:

$$G(k_x, k_y) = e^{-i(k_x \text{ x-center} + k_y \text{ y-center})} F(k_x, k_y).$$

X-center and y-center are the coordinates of the center of the object. If the object is rotated at an angle ß to the x-axis then its Fourier transform is computed by using the same equations as above but by first transforming the coordinates onto a new set of axes rotated at the angle ß. The equations for coordinate transformation are:

$$k_x' = k_x \cos ß + k_y \sin ß$$
$$k_y' = -k_x \sin ß + k_y \cos ß.$$

Finally the signal from each object is attenuated to account for T_2 decay. The total signal is the sum of the signal from each object within the phantom. The signal is passed to a 2-dimensional fast Fourier transform routine for inversion and display. The simulation package used the following parameters and assumptions in generating images.

Parameters:
-Imaging area: 20x20 centimeters.
-Gradients: .25 gauss/centimeter.
-Echo Time (TE): 28 milliseconds.
-Images: 256 x 256 pixels.
-All images are magnitude images.

Assumptions:
-Perfect π pulses.
-Inhomogeneities are static throughout acquisition and are small compared to gradients.

The phantom used in the simulation is shown in figure 9. The software used to generate the phantom was originally developed for simulation studies of Positron Emission Tomography[11]. T_2 values for the phantom ranged from 45 to 100 milliseconds. These values are consistent with those in biological samples[12]. In the letters "N","M","R" $T_2 = 75,100,45$ milliseconds respectively. T_2 for the ellipses in the lower left, center, and upper right portions of the phantom are 75, 45, and 100 milliseconds respectively. The simulation distorts and attenuates different parts of the image by different amounts corresponding to the local values of T_2. That is, each object in the phantom has its own transfer function consistent with its own value of T_2. However, in all objects the shape of the transfer function is the same; an exponential

in both the k_x and k_y directions. T_2 simply determines the value of the decay constants in equations [4] and [5].

FIGURE 9
Phantom

Intensity is proportional to the density of magnetic spins. T_2 varies throughout phantom. Letters "N","M","R" T_2 =75,100,45 milliseconds respectively. Ellipses lower left, center, and upper right T_2 =75, 45, 100 milliseconds respectively.

RESULTS

As shown in figure 10, the simulation package was used to generate the transfer function, the point spread function (PSF), and the image for 2, 4, and 8 echo PERME imaging and spin-warp imaging. In each case the PSF was generated by Fourier inversion of the transfer function. That is, the PSF is the impulse response. A T_2 of 50 milliseconds was assumed in generating the PSFs from the transfer functions.

Since both PERME and spin-warp imaging use a y-readout gradient, differences between the two methods are only in the x direction. Thus the transfer functions and PSFs shown in figure 10 are the profiles in the x direction only. Because the PERME transfer function is exponential the magnitude of its Fourier transform, the PSF, resembles the Lorentzian line shape well known to spectroscopists.

The images of figure 10 show that part of the "N" of the phantom is folded over into three corners inappropriately. This was shown intentionally to demonstrate the effect of inadequate sampling. The imaging parameters were selected to sample a 20x20 centimeter imaging area. However the phantom was created with part of the "N" lying outside of the imaging area. As a result part of the "N" gets wrapped around to the other corners. To avoid this aliasing, k-space needs to be sampled more finely in both the k_x and k_y directions.

A comparison of the four images of figure 10 shows that PERME imaging has more T_2 contrast than the spin-warp image. In addition the 2 and 4 echo PERME sequences reveal virtually no artifacts.

Figure 11 shows the effect of two proposed methods which also use multiple echoes to sample multiple lines in each FID. The first method samples sequential lines in each FID. That is, k-space lines 1,2,3,4 are sampled in FID-1. Lines 5,6,7,8 are sampled in FID-2. Four adjacent lines are sampled in each successive FID. The second proposed method only uses the phase encoding gradient twice in sampling 4 lines in each FID. The method utilizes the Hermitian symmetry of the Fourier domain by sampling complex conjugate lines in echoes 1 and 2 and a second pair in echoes 3 and 4. That is for a 16x16 image, lines 1,16,2,15 are sampled in of echoes 1,2,3,4 respectively of the first FID. Lines 3,14,4,13 are sampled in the second FID. Thus in each FID the phase encoding gradient is only needed before the first and third π pulses. The images in figure 11 demonstrate that these two proposed methods yield unacceptable artifacts.

Figure 12 demonstrates the effect of two methods which have sampling orders similar to PERME imaging but which do not utilize timing delays. The images associated with these methods have a blurring artifact.

DISCUSSION

Results shown in figure 10 indicate that the exponential transfer function of PERME imaging yields images without artifacts when a two or four echo sequence is used. The exponential shape was desired so that artifacts would be minimized and would be of the same form as in the y direction. (Recall that the k_y transfer function profile is also exponential.) The T_2 contrast of the PERME method is a result of the fact that data sampling occurs over an effective time of n+1 echoes. For example, when four echoes are used, the first data point is sampled at the beginning of the first echo of FID-1. The last data point is collected at the end of the fourth echo of FID-64. However the 64th FID has a total delay of one TE. Thus, T_2 differences have an effective time of five echoes in which to manifest themselves.

Figure 11 demonstrates very effectively the importance of the strategy used in mapping k-space. The transfer function must be considered in choosing a k-space trajectory. The extreme artifacts of figure 11 are due to the very jagged transfer functions associated with these two naive methods for mapping multiple lines of k-space in a single FID. Figure 12 also demonstrates the effects of k-space trajectories. The methods shown have a non-sequential sampling strategy similar to the PERME method but do not have timing delays. The lack of timing delays causes the four discontinuities in each transfer function . The blurring in the images is due to the high-frequency power associated with the step-like transfer functions. Thus it is clear that both the non-sequential sampling and the timing delays are essential factors in the potential success of PERME imaging.

An analysis of noise has not been considered here. It is clear that PERME imaging will suffer from noise distributed among the various spatial frequencies as will any other imaging scheme. The differences between imaging schemes in signal-to-noise ratio (SNR) for various spatial frequencies is dependent only on the amount of attenuation. The attenuation is described by the transfer function. As mentioned above, PERME imaging inherently attempts to equalize the transfer function for all frequencies by sampling complex conjugate pairs early and late in T_2 decay. Nonetheless PERME imaging is limited by SNR considerations. If not one would simply use n echoes to collect n lines of k-space data to produce an nxn image. However as T_2 relaxation continues spatial frequency data eventually becomes dominated by noise. It is likely that four echoes will be the limit in practice (assuming echo times on the order of 20 to 30 milliseconds). Thus, the improvement in speed will be a factor of four over spin-warp imaging. As discussed above, the total data sampling time causes PERME imaging to have a long effective echo time. The same effect is expected to cause the differences in SNR between different parts of the image, with different T_2s, to be more dramatic than that of spin-warp imaging.

CONCLUSIONS

This paper has shown the ease in which k-space analysis can be used to compare and contrast various imaging schemes. The new PERME method is a new k-space trajectory strategy which can be considered as a hybrid between projection techniques and echo-planar techniques. As evidenced by the images of figure 10 the exponential transfer function of PERME imaging is favorable over other methods evaluated. The PERME method features the high-resolution associated with other current methods while decreasing the total number of FIDs required.

It is interesting to consider the possibility of combining PERME imaging with other high-speed sequences. Of particular interest is the fast Fourier trajectory of Van Uijen et al.[13] in which several adjacent lines of k-space are sampled in a single echo. In this method the phase-encoding gradient is active both prior to and during acquisition when the spins are also precessing under the influence of the readout gradient. During readout the phase-encoding gradient is modulated so that adjacent lines of k-space are traversed in a single echo. In the limit of large modulations and a small readout gradient this method approaches the echo-planar technique. PERME imaging could easily be extended to incorporate this modulation of the phase-encoding gradient. Thus, in a single FID multiple lines would be sampled in each of multiple echoes. If, for example, a two echo PERME sequence incorporated a four line fast Fourier trajectory then total imaging time would be decreased by a factor of eight over the standard spin-warp method. A four echo PERME/four-line fast Fourier sequence would decrease imaging time by 16.

It is clear that because no new hardware nor software is required, implementation of the PERME method with or without incorporating other strategies is straightforward. For these reasons PERME imaging could prove to be of great use in the production of everyday NMR images at speeds greatly reduced from that of spin-warp imaging yet without sacrificing quality.

REFERENCES

[1]   P. Mansfield, Journal of Physical Chemistry 10, L55 (1977).

[2]   D. Twieg, to be published, Magnetic Resonance in Medicine 2, (1985).

[3]   W. Edelstein, J. Hutchinson, G. Johnson, and T. Redpath, Physics in Medicine and Biology 25, 751 (1980).

[4]   P. C. Lauterbur, Nature 242, 190 (1973).

[5]   A. Kumar, D. Welti, and R. Ernst, Journal of Magnetic Resonance 18, 69 (1975).

[6]   W. S. Hinshaw, Journal of Applied Physics 47, 3709 (1976).

[7]   D. Twieg, Medical Physics 10, 5 (1982).

[8]   K. F. King and P. R. Moran, Medical Physics 11, 1 (1984).

[9]   S. J. Ljunggren, Journal of Magnetic Resonance 54, 338 (1983).

[10]   Z. H. Cho, Proceedings of the IEEE 70, 10 (1982).

[11]   R. H. Huesman, G. T. Gullberg, W. L. Greenberg, and T. F. Budinger, Donner Algorithms for Reconstruction Tomography, Lawrence Berkeley Labratory, Publication PUB-214, (1977).

[12]   P. Bottomley, T. Foster, R. Argersinger, and L. Pfeifer, Medical Physics 11, 4 (1984).

[13]   C. M. J. Van Uijen, J. H. Den Boef, and F. J. J. Verschuren, Magnetic Resonance in Medicine 2, (1985).